An Optode Sensor Array for Long-Term In Situ Oxygen Measurements in Soil and Sediment

L. F. Rickelt,* L. Askaer, E. Walpersdorf, B. Elberling, R. N. Glud, and M. Kühl

Long-term measurements of molecular oxygen (O_2) dynamics in wetlands are highly relevant for understanding the effects of water level changes on net greenhouse gas budgets in these ecosystems. However, such measurements have been limited due to a lack of suitable measuring equipment. We constructed an O_2 optode sensor array for long-term in situ measurements in soil and sediment. The new device consists of a 1.3-m-long, cylindrical, spear-shaped rod equipped with 10 sensor spots along the shaft. Each spot contains a thermocouple fixed with a robust fiberoptic O_2 optode made by immobilizing a layer of Pt(II) meso-tetra(pentafluorophenyl) porphine in polystyrene at the end of a 2-mm polymethyl methacrylate plastic fiber. Temperature and O_2 optode readings are collected continuously by a data logger and a multichannel fiberoptic O_2 meter. The construction and measuring characteristics of the sensor array system are presented along with a novel approach for temperature compensation of O_2 optodes. During in situ application over several months in a peat bog, we used the new device to document pronounced variations in O_2 distribution after marked shifts in water level. The measurements showed anoxic conditions below the water level but also diel variations in O_2 concentrations in the upper layer presumably due to rhizospheric oxidation by the main vegetation *Phalaris arundinacea*. The new field instrument thus enables new and more detailed insights to the in situ O_2 dynamics in wetlands.

Molecular oxygen (O_2) is a key environmental parameter in most ecosystems, where its concentration and dynamics not only outline the activity and distribution of aerobic processes but also provide a proxy for overall biogeochemical carbon fixation and mineralization (Glud, 2008). Measurements of O_2 transport and dynamics in organic soils and sediments are central for estimating the consequences of spatio-temporal water level fluctuations because decomposition of subsurface carbon pools and the resulting emissions of the greenhouse gases CO_2, CH_4, and N_2O are strongly affected by the O_2 availability (Askaer et al., 2010; Jørgensen et al., 2012; Liengaard et al., 2013). For example, in peat soil, O_2 is the primary factor controlling subsurface CH_4 dynamics (Megonigal et al., 2003). A deeper understanding of how O_2 supply is related to water level regimes is therefore of primary interest when assessing CH_4 emissions to the atmosphere, especially in relation to the possible consequences of hydrological changes in a global change perspective, be it sea level rise affecting shallow coastlines and estuaries, increased rainfall intensity causing flooding events, or increased draught periods causing water level draw down (IPCC, 2007).

The water level is a primary control of subsurface O_2 availability due to low O_2 solubility and an approximately 10^4 times slower O_2 diffusion in water as compared with air. Spatio-temporal changes in O_2 concentration and dynamics are not well understood, and there is a need for a continuous high-resolution monitoring of O_2 dynamics in situ. Numerous studies have investigated water table effects on CH_4 emissions (e.g., Macdonald et al., 1998; Daulat and Clymo, 1998; Hargreaves and Fowler, 1998; Kettunen, 2003; Schäfer et al., 2012). Also, the complex interactions of subsurface O_2 concentrations with CH_4 production and consumption have been demonstrated in a laboratory study (Askaer et al., 2010). Besides a field study linking subsurface O_2 and CH_4 concentrations (Elberling et al., 2011), to our knowledge

J. Environ. Qual. 42:1267–1273 (2013)
doi:10.2134/jeq2012.0334
Received 2 Sept. 2012.
*Corresponding author (lfrickelt@bio.ku.dk).

L.F. Rickelt and M. Kühl, Marine Biological Section, Dep. of Biology, Univ. of Copenhagen, Strandpromenaden 5, DK-3000 Helsingør, Denmark; L. Askaer, E. Walpersdorf, and B. Elberling, Dep. of Geosciences and Natural Resource Management, Univ. of Copenhagen, Øster Voldgade 10, DK-1350 Copenhagen K, Denmark; B. Elberling, Center for Permafrost (CENPERM), Univ. of Copenhagen, Øster Voldgade 10, DK-1350 Copenhagen K., Denmark; R.N. Glud, Univ. of Southern Denmark & Nordic Center for Earth Evolution–NordCEE, Odense, Denmark, Scottish Association for Marine Science (SAMS), Marine Laboratory Dunstaffnage, Oban, Argyll PA37 1QA, Scotland, UK, and Greenland Climate Research Center, Greenland Institute of Natural Resources, Nuuk Greenland; M. Kühl, Plant Functional Biology and Climate Change Cluster, Univ. of Technology Sydney, P.O. Box 123, Ultimo Sydney NSW 2007, Australia, and Singapore Centre on Environmental Life Sciences Engineering, School of Biological Sciences, Nanyang Technological Univ., Singapore. Assigned to Associate Editor Søren O. Petersen.

Abbreviations: POF, polymethyl methacrylate optical fiber.

continuous O_2 measurements in situ have not been available to support the interpretation of CH_4 emissions.

Optical oxygen sensors (i.e., O_2 optodes) are well suited for environmental monitoring due to their mechanical robustness and good long-term stability of measuring signals (Kühl, 2005; Holst et al., 2000). Fiberoptic O_2 sensor arrays have previously been described for microscale measurements of O_2 distribution (Holst et al., 1997; Glud et al., 1999; Fischer and Koop-Jakobsen, 2012) and for measurements in soil and sediment (Hecht and Kölling, 2001; Kölling et al., 2002). These systems did not include temperature compensation. Here, we present a robust optical O_2 sensor array enabling long-term in situ deployment and continuous monitoring of O_2 penetration and temperature on a time scale of several months. The construction, measuring characteristics, and temperature compensation of the new instrument are described, together with an example of in situ application in a peat soil.

Materials and Methods

Construction of the Sensor Array

The sensor array was built into a cylindrical spear (Fig. 1) made of polyethylene (1200 mm length, 50 mm outer diameter, and a wall thickness of 5 mm). Along the cylinder shaft, 10 holes (8 mm in diameter) were drilled at distances consistent with measuring depths of 2, 5, 10, 20, 30, 40, 50, 60, 70, and 80 cm when the spear is placed at an angle of 30° relative to a vertical position and with 200 mm of the spear above the sediment/soil surface. A 4-mm-deep countersink with a 20-mm-diameter was cut around each hole for the placement of a bolt to fix the sensors (see below). A hole (20 mm diameter) was drilled 50 mm from the top and used for joint sensor connection to a data logger. Each of the 10 combined O_2 and temperature sensors was constructed and mounted in the following way.

Two holes (2.1 mm diameter) were drilled in each of 10 steel screw bolts (8 × 20 mm) lengthwise from the head. One hole was drilled through, and the other stopped 0.5 mm from the bottom. The bolts were then fixed with a sealant (Loctite, Henkel Norden) to a stainless steel bar (3 mm × 16 mm × 905 mm) with 10 8-mm holes corresponding to the holes in the cylinder shaft, and 10-mm silicone disks were placed on each bolt thread. The soft silicone made it possible to tighten the outer nuts flush with the bolt ends and the shaft surface when the system was assembled. The disks also function as spacer between the steel bar and the shaft.

A welded-tip thermocouple (Type T, PTFE Insulated, Z2-T-2M, Labfacility Ltd.) and the sensing end of a 5-m-long plastic polymethyl methacrylate optical fiber (POF) (step index, 2 mm diameter, with a polymethyl methacrylate core and a fluorinated polymer cladding; Laser Components GmbH) were mounted in each steel screw with two-component epoxy resin (Fig. 1). The thermocouple and fiber were held together by 3.2-mm heat-shrinkable tubing (Low Shrink Temperature polyolefin tubing; Farnell), leaving 3 cm free at both ends.

The steel bar was pushed into the shaft, and the bolts were tightly fixed with 5-mm nuts and polyurethane rubber (Sikaflex-11FC, Sika A/S) through the side holes of the spear. The detector ends of each thermocouple and fiber pair was pushed out through the 20-mm hole at the top of the sensor array shaft. After polishing, each POF fiber end was mounted in a SMA-connector (Laser Components GmbH) enabling connection to a fiberoptic O_2 meter.

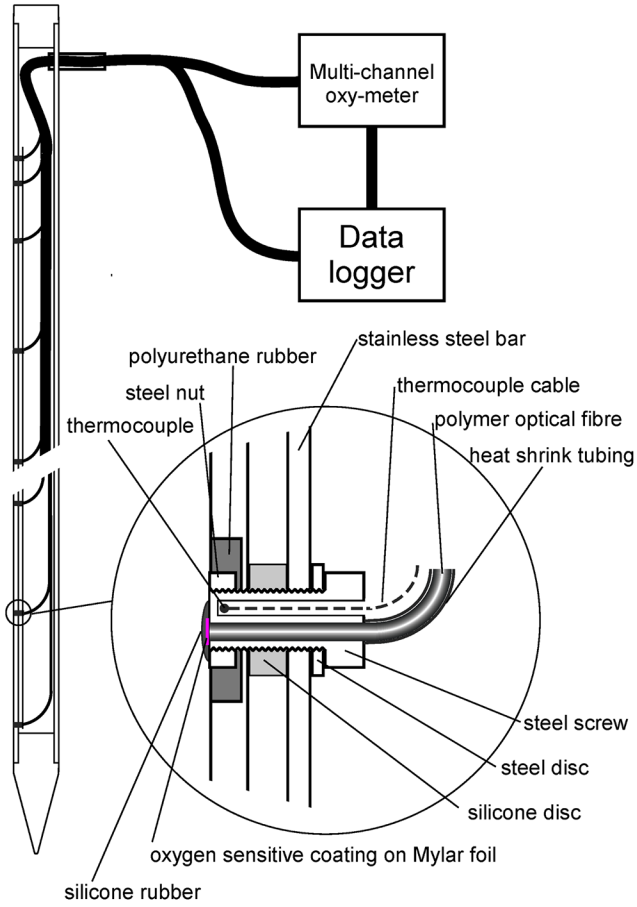

Fig. 1. Schematic drawing of the O_2 and temperature sensor array spear and the connection of sensors to the data logger.

A disk of a transparent and O_2–impermeable carrier foil coated with O_2 sensor chemistry (diameter, 2.5 mm; thickness, 0.125 mm) (sMylar, Goodfellow Cambridge Ltd.) was glued with UV curing resin (Dymax) onto the measuring end of the POF at the outer surface of the steel screw. Gluing the sensor foils to the measuring end of the POF ensured a durable and efficient optical coupling of the sensor layer luminescence into the POF. The disk was prepared with a drop of a 3.3% (w/w) solution of an O_2 sensor chemistry cocktail consisting of 25 mg Pt(II) meso-tetra(pentafluorophenyl)porphine (Frontier Scientific, Inc.), 1 g polystyrene (Goodfellow Cambridge Ltd.), and 0.5 g TiO_2 in chloroform. After evaporation of the sensor cocktail solvent, each sensor spot was knife-coated by a thin layer of highly O_2 permeable black silicone (Elastosil N189, Wacker-Chemie GmbH) to seal it flush with the shaft of the array. The spatial resolution of the O_2 sensors is estimated to be approximately 2.5 mm (the fibers are 2 mm), and the spatial resolution of the temperature sensors is estimated to be approximately 10 mm (the steel bolts are 8 mm).

The lower-most end of the sensor array spear was closed with a 100-mm conical tip, and the top of the cylinder was closed with a 20-mm cylinder, both made of solid PVC and equipped with a 40 mm plug. The sensor array was filled with clean sand. In the field, all sensor signals were acquired by a data logger (CR1000, Campbell Scientific Ltd.). Thermocouples were connected directly to the data logger, whereas the O_2 optodes were connected to a multichannel fiberoptic meter (OXY-10, Presens GmbH) interfaced to the data logger. The instruments were powered by

220V in the laboratory and during in situ field measurements. We evaluated the O_2 optodes with respect to performance, temperature response, and response time. These measurements were done with the OXY-10 meter or with a single channel version with similar measuring characteristics (FIBOX-3, Presens GmbH).

Performance of the Oxygen Optode

Oxygen optode measurements can be based on measuring O_2–dependent changes in the intensity or decay time (also called lifetime) of specific luminescent indicator dyes that are quenched by O_2 (Kühl 2005). Luminescence lifetime-based measurements are more robust and less prone to optical artifacts than luminescence intensity-based O_2 measurements (Holst et al., 1995, 2000). The fiberoptic O_2 meter used in this study measures the luminescence lifetime with a phase-modulation technique (Holst et al., 1995). When the luminescent O_2 indicator is excited with sinusoidally intensity-modulated light (at frequency, f_{mod}), the lifetime of the indicator causes a time delay of the emitted red-shifted luminescence; this delay is called the "phase angle" (Φ) between the excitation and the emitted signal. The lifetime, τ, is calculated from the measured phase angle as:

$$\tan(\Phi) = 2\pi \cdot f_{mod} \cdot \tau \quad [1]$$

As shown in earlier work, reviewed by Holst et al. (2000) and by Kühl (2005), the response of POF-based O_2 optodes follows a modified Stern-Volmer relation that includes a nonquenchable fraction, α:

$$\frac{\tan(\Phi_c)}{\tan(\Phi_0)} = \frac{I_c}{I_0} = \frac{\tau_c}{\tau_0} = \frac{1-\alpha}{1+K_{SV}\cdot c} + \alpha \quad [2]$$

where Φ_0, I_0, and τ_0 are the phase angle, luminescence intensity, and lifetime, respectively, of the indicator in the absence of O_2, and Φ_c, I_c, and τ_c are the phase angle, luminescence intensity, and lifetime of the indicator at a given O_2 concentration, c. K_{SV} is a characteristic quenching coefficient of the immobilized indicator. For a given mixture of indicator and matrix material, α is usually temperature independent and constant over the dynamic range of the optode (Kühl, 2005), and Eq. [2] accurately describes the nonlinear behavior of I or τ vs. O_2 content. The nonquenchable fraction, α, and K_{SV} can be determined from measurements of luminescence intensity or lifetime under at least three defined O_2 contents (e.g., 0, c_1 = 100% air saturation, and c_2 = 20% air saturation) (see details in Kühl [2005]). Once α has been determined, the calibration of the optical O_2 sensor can be done by a simple two-point calibration (e.g., measurements at zero O_2 and at a known O_2 content), typically water at atmospheric saturation at experimental temperature and salinity.

We had originally placed the O_2 sensing material directly on the end of the POF, which yielded a mechanically robust sensor as only 1 sensor out of 10 lost its signal over a 7-mo pilot deployment period. However, with this type of direct immobilization, the chloroform in the O_2 sensor chemistry cocktail dissolved some of the POF material, causing a relatively high nonquenchable fraction (i.e., α = 0.415 ± 0.002 [mean ± SD]; n = 3). Instead, the O_2 indicator layer was cast onto a transparent carrier foil, which could be attached onto the POF using UV-curing glue. This type of immobilization yielded α values typical of planar (2D) optodes (i.e., $\alpha \sim 0.11$) (Kühl and Polerecky, 2008), and it was simpler to manufacture such sensors reproducibly while retaining good mechanical robustness. This immobilization method was therefore used in the final design of the sensor array spear.

Calibration and Temperature Response of Oxygen Optodes

We quantified the temperature dependency of all 10 sensors in the array. The luminescence lifetime, and with it Φ and K_{SV}, depend on temperature. Optode sensors show a linear decrease in $\tan(\Phi)$ with increasing temperature, T, which in the relevant temperature interval (0–25°C) can be described by:

$$\tan(\Phi)_T = \tan(\Phi)_0 + d \cdot T \quad [3]$$

where d is the slope and $\tan(\Phi)_0$ is the intercept of the curve with the y axis at 0°C, and $(\Phi)_T$ is the phase angle at temperature T. Using Eq. [3], the temperature dependency of K_{SV} can be described as:

$$K_{SV}(T) = \left\{ \frac{1-\alpha}{\left[\frac{\tan(\Phi_1)_0 + d_1 \cdot T}{\tan(\Phi_0)_0 + d_0 \cdot T}\right] - \alpha} - 1 \right\} \cdot \frac{1}{c_1} \quad [4]$$

The anoxic calibration and the corresponding measurement of temperature response of the optodes were performed in the following way. The spear was placed in a water-filled cylindrical container (length, 115 cm; diameter, 19 cm) in a temperature-controlled room at approximately 4°C. For removal of O_2, 200 g sodium dithionite (technical grade; Struers) was dissolved to a final concentration of 0.75%. The solution was kept anoxic by continuous flushing with N_2 gas (using a pumice stone) for 2 d, and then the system, including the N_2 flushing, was transferred to a 21°C room. The sensors were immediately connected to the OXY-10 fiberoptic O_2 meter, and the O_2–dependent phase angles of each sensor were recorded every 15 s during the warm-up period. The water temperature was measured continuously with an Omnitherm Pt 100 Digital Thermometer (RS components). The experiment was interrupted when the water temperature reached 16.7°C due to depletion of the N_2 supply.

Calibration and temperature responses in 100% air saturated water were determined in a similar way. The container was filled with water and flushed with ambient air. The system was left for 2 d to equilibrate. After a first measurement at ~4°C in the cold room, the system was moved to the 21°C room, while still flushing with air. The water temperature reached 20.5°C after 24 h, and the experiment was stopped.

In principle, increasing hydrostatic pressure in the calibration container could affect sensor readings due to the combined pressure effect on sensor materials and the O_2 solubility in the water (Uchida et al., 2008). However, detailed measurements with a single optode done at 10-cm intervals throughout the well mixed calibration chamber did not reveal any difference in phase angle. Apparently, the difference in signal caused by hydrostatic pressure differences was below the sensitivity level of these sensors. Hydrostatic pressure effects in situ were negligible due to the shallow O_2 penetration in the peat soil.

Response Time of Oxygen Optodes

Response time measurements of the sensor array were performed at 20°C. A cylindrical container (length, 120 cm; diameter, 12 cm) equipped with a pumice stone at the bottom was used in this case. The container was filled with water and flushed with air to obtain atmospheric saturation, and sodium sulfite (Merck) was added to the water (final concentration, 1%) together with continuous flushing with N_2 to induce anoxic conditions while continuously logging the O_2–sensor response at 15-s intervals. Water temperature was monitored continuously. Separate measurements with a fast-responding micro-optode (Klimant et al., 1995) were included for reference.

In Situ Application

In situ O_2 measurements were initiated in November 2008 in a peat soil within the wetland area Maglemosen located 20 km north of Copenhagen, Denmark (55°51′ N; 12°32′ E). The peat soil in this area is subject to fluctuations in water level within the upper meter but maintains moist surface conditions year-round. Water level increases are induced by precipitation events resulting in water percolation from above and lateral flow from elevated surroundings. Water level was measured at 10-min intervals with a barometer-compensated pressure transducer (PCR 1830 series, Druck, ThermX) (Jørgensen et al., 2012). The transducer wire was attached to a horizontal bar, and the transducer head was submerged in a 2-m-long perforated plastic tube placed in a sand cast drill hole. The horizontal bar was mounted with 3-m-long stainless steel rods inserted into the underlying mineral soil to avoid potential errors caused by seasonal displacement of the surface after shrinkage and swelling of the peat soil.

The spear was inserted into a predrilled hole (48 mm diameter) and with the measuring spots pointing downward to reduce any effects of lateral preferential flow. The O_2 content was measured continuously at 10-min intervals at all 10 depths. The O_2, temperature, and water level measurements were logged with the CR1000 data logger. For illustration, we present soil O_2 contents at the 10 depths during a 3-wk period in spring (12 May to 1 June 2009).

Results and Discussion

Evaluation of Optode Sensor Array Performance

Our measurements showed a linear change in tan(Φ) (and thus the luminescence lifetime) vs. increasing temperature T (in °C) in accordance with Eq. [3], both under anoxic (Fig. 2A) and air saturated conditions (Fig. 2B) and with similar slopes among 10 sensors (R^2 > 0.99 [slope = −0.00424 ± 0.00016; n = 10] and R^2 > 0.99 [slope = −0.00338 ± 0.00017; n = 10] for anoxic and air saturation, respectively). The variation of K_{SV} with temperature was calculated by Eq. 4 from the temperature calibrations of the 10 sensors (Fig. 2C). Thus, it is possible with a good approximation to transform the two calibration values for each sensor done at a given temperature to calibration values at other temperatures using the slopes derived from the anoxic and the air-saturated system. Using such calculated calibration values, it becomes in principle possible to calculate the O_2 content from phase angle data measured at temperatures of 0 to 25°C using Eq. [4]. Unpublished experimental results with similar sensors have shown that the relationship between tan(Φ) and temperature

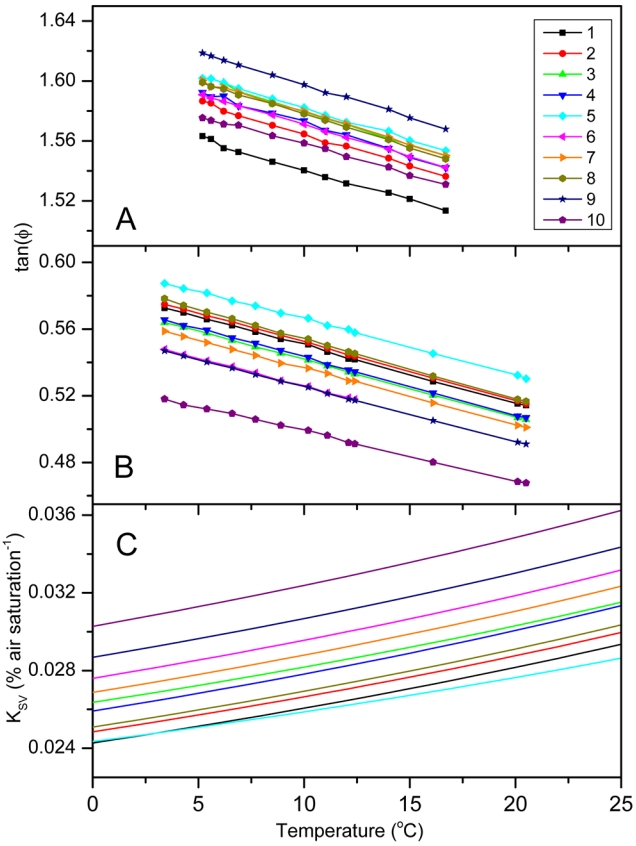

Fig. 2. Temperature response of 10 optical O_2 sensors, quantified as the O_2–dependent luminescence lifetime proportional tan(Φ) with sensors in anoxic water (A) and in water at 100% atmospheric saturation (B). Stern-Volmer quenching constant K_{SV} (see Eq. [3]) vs. temperature for each optical O_2 sensor (C).

is not completely linear from 0 to 80°C, although it is safe to assume linearity in 25°C intervals. The thermocouples were calibrated at 4 and 21°C (Jørgensen et al., 2012).

Separate measurements with a fast-responding micro-optode showed that anoxic conditions had developed within 30 s. The average 90% response time of the O_2 sensors of the array was 255 ± 58 s (Fig. 3; n = 10). This relatively slow operational response time was due to the use of a rather thick indicator layer combined with a relatively thick silicone coating conferring strong mechanical stability. Response times of a few seconds could be obtained by reducing the thickness of the indicator and the silicone coating, which would potentially compromise the mechanical stability. However, for the long-term in situ measurements reported here, where diel to seasonal changes of soil O_2 levels were to be monitored, a response time of several minutes was adequate.

Monitoring Site Characteristics

Earlier studies have reported marked spatial variability in peat characteristics over the depth range, where the water table typically fluctuates (Askaer et al., 2010). These peat characteristics, in combination with plant-mediated subsurface O_2 transport, regulate the actual net transport and depth distribution of oxygen in the root zone (Elberling et al., 2011; Askaer et al., 2011). Although the water level typically varied from 0 cm to several cm above the soil surface during winter to approximately 50 cm below in the driest summer period, the water level ranged from 12 to 41 cm below the soil surface in the

selected 3-wk measurement period. During this time, the water level declined, although precipitation events during the period resulted in transient rises in water level (Fig. 4).

At the monitoring site, the organic material in the top 0.6 m of the peat soil has been deposited in a freshwater lake, turning the lake into a moist wetland (Askaer et al., 2010). Soil auger cores (0–120 cm) showed that peat depth was fairly uniform throughout the wetland independent of surface vegetation. Three contrasting layers were observed. The top approximately 25 cm consisted of recognizable plant parts and fresh plant litter. At 26 to 60 cm depth, the peat became increasingly humified and darker in color, indicative of silty detritus deposited in a fresh water environment. At approximately 60 cm depth, there was an abrupt change in the sediment from peat to carbonate-rich organic silt. This layer extended to approximately 80 cm below the surface, with a few thin dark layers of peat. Bulk density increased from 0.2 to 0.3 g cm^{-3} in the upper 10 cm to 0.4 g cm^{-3} at 40 to 50 cm depth, coinciding with a decrease in porosity and apparent diffusivity. This indicated decreasing hydraulic conductivity and increasing water retention with depth (Boelter, 1965), in particular below the main root zone (0–25 cm depth).

Oxygen Conditions in the Peat Soil Profile

Below the active root depth of the dominant vegetation type (*Phalaris arundinaceae*), O_2 supply is limited by molecular diffusion under saturated conditions (Askaer et al., 2010, 2011; Jørgensen et al., 2012). In general, O_2 distribution in the peat soil was strongly affected by water level. When the water level reached below a specific sensor depth, the local O_2 content increased, and vice versa. The sensors at 50 cm depth and below showed anoxia (<1% air saturation) throughout the measuring period. At 40 cm depth, the O_2 content was <1% air saturation until the water level dropped below this depth by the end of May, resulting in a maximum O_2 concentration of 11% air saturation on 1 June (Fig. 4A, lower right hand corner). At 30 cm depth, the O_2 content was constant at <1% air saturation until 22 May. Subsequently, it momentarily increased to 5% air saturation in response to a rapid water level decline reaching the sensor measuring depth in the horizon. On 25 May, the water level again dropped below the 30 cm sensor, resulting in a rapid increase in O_2 availability in the range of 50 to 65% air saturation. On 29 May, the water level rose to 10 cm above the sensor for a 2-d period, resulting in a decrease in O_2 content to <1% air saturation before rapidly rising to 55 to 65% air saturation. At 20 cm depth, the water level declined below the sensor on 15 May for a 2-d period, resulting in an increase in O_2 content up to 43% air saturation, although it rapidly decreased to <1% air saturation when the water level increased. As the water level decreased for a longer period of time, around 20 May, the O_2 content increased steadily until reaching stability around 28 May at 80% air saturation.

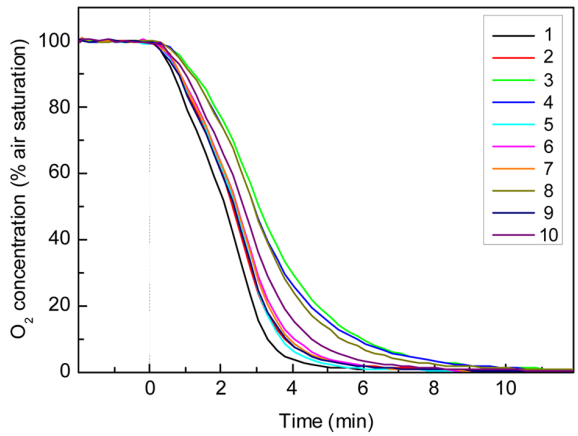

Fig. 3. The response time of the 10 calibrated fiberoptic minisensors used in the sensor array spear upon a shift from air saturated to anoxic water at 20°C.

The water level did not increase above the O_2 sensor at 10 cm depth. Still, an unexpected decrease in O_2 content to 53% air saturation was observed on 18 May in response to precipitation events on 16 May (3.4 mm), 17 May (0.7 mm), and 18 May (1.0 mm) after a period without precipitation. It took roughly 5 d to re-establish stable O_2 contents around 83% air saturation. This is consistent with the lack of reaction of the 20-cm sensor during 18 to 21 May, where the water level measurements showed a level below this sensor.

The O_2 contents at the 2- and 5-cm depths were very similar. At these depths, the soil was continuously oxic, with O_2 contents of 87

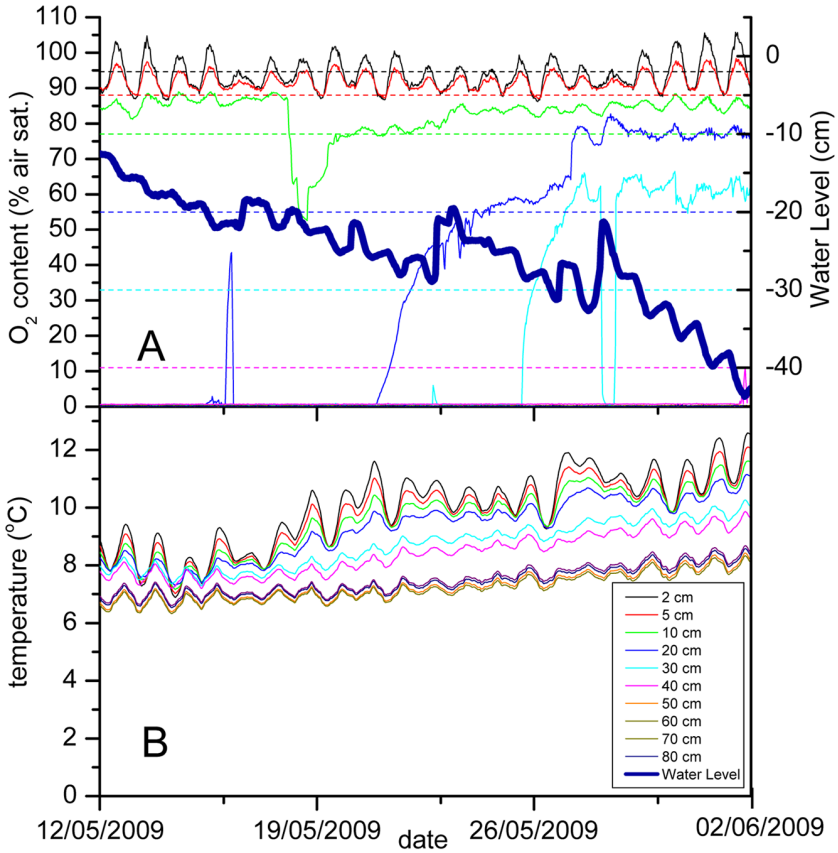

Fig. 4. In situ measurements in a peat soil (Maglemosen, Denmark) during a 3-wk period in 2009. (A) Oxygen and water level variations. The dashed lines mark the depths of the respective O_2 sensors in relation to the water level. (B) The measured temperature at the same depths.

to 105% (mean 93.9%) air saturation at 2 cm depth and 88 to 98% (mean, 91.9%) air saturation at 5 cm depth. The high O_2 content was due to the fact that the water level did not reach above these probes during the monitoring period reported here. Apparently, O_2 diffusion from the atmosphere was effective at replenishing microbial O_2 consumption. These near-surface sensors exhibited diel O_2 variations, with O_2 contents above 100%. Rhizospheric oxidation by the dominating wetland plant *Phalaris arundinacea* could be a possible explanation for the diel variations in O_2 content of the uppermost soil layers (Askaer et al., 2011; Jørgensen et al., 2012). We have obtained preliminary data on O_2 dynamics in the *Phalaris* rhizosphere as monitored in 2D with planar optodes (Liengaard et al., unpublished data), but a more detailed discussion and comparison of the new spear system for O_2 measurements with planar optodes is outside the scope of this paper.

The high water storage capacity of fresh peat and its ability to shrink and swell in accordance with available moisture minimize water level fluctuations and maintain the water table below (but close to) the surface (Ingram, 1983). Such shrinking and expansion can affect other parameters, such as soil bulk density, water retention, hydraulic conductivity, and, consequently, gas diffusion and O_2 distribution (Elberling et al., 2011). However, we can only speculate on the importance of such effects on our field data because we did not monitor the shrinking and swelling of peat at the field site.

Variability of Oxygen Distribution

The O_2 conditions in wetland soils under varying water saturation levels are complex, and few studies have attempted to document O_2 dynamics in such systems at high spatiotemporal resolution. A study of the effect of small-scale peat soil structure on O_2 availability (Askaer et al., 2010) found vast soil heterogeneity and the presence of oxic zones below the water level in periods up to days after water saturation. This was presumably due to wetting inhibition combined with air inclusion, the formation of water-repelling film, and alterations of pore structure due to shrinkage during the drained period (Schwärzel et al., 2002). Anoxic zones were also observed above the water level (Askaer et al., 2010). These observations suggest a discontinuous soil pore system. During diel temperature variations, discontinuous pores could experience pressure changes potentially affecting the partial pressure and thus the measured O_2 content. With the diel temperature variations of <3°C, this possible error is estimated to be insignificant.

Two-dimensional O_2 imaging with planar O_2 optodes in peat from the same wetland area has previously demonstrated a large spatial variation at the mm scale (92 ± 5% air saturation when fully waterlogged with oxygenated water) within the surface layers of the soil profile (Askaer et al., 2010). The sensor array described here measures exclusively in one point at each depth, and although pronounced cyclic variations were seen, the highest diurnal variations were within the same range as the spatial variation (e.g., 94.1 ± 5.6% air saturation on 13 May).

Temperature and Oxygen Dynamics

Figure 5 shows detailed O_2 and temperature readings for the sensors at the 2-, 5-, and 10-cm depths over the first 3 d of the monitoring period. Soil temperature showed an increase from the morning until sunset and a subsequent decrease during the night, whereas the O_2 content had a maximum shortly after noon, when the photosynthetic activity was presumably highest, and then decreased until the next morning.

For the upper 10 cm, diel variations of the measured temperature and O_2 levels did not coincide. The O_2 levels showed a very regular and constant diel variation, reaching a maximum close to noon, which was 11 ± 4% higher (at 2 cm) than the minimum O_2 level measured 0 to 3 h after midnight. The daily average temperature increased over the same 3-wk period, and the diel temperature variations in the top 2 cm were less regular, with a minimum between 07:00 and 10:00 and a maximum between 19:30 and 22:30 (Fig. 4). At 2 cm depth, the difference between the daily minimum and maximum temperatures was 1.4 ± 0.6°C. At 100% air saturation, a 1°C temperature difference typically gives a change in O_2 optode signal equivalent to <2% air saturation. The variations of in situ temperature were thus far too small to have a significant effect on the O_2 measuring signals even if the sensors were not temperature corrected. Because the sensors were temperature corrected and the temperature variations were out of phase with the observed O_2 fluctuations, we rule out the possibility that the observed O_2 fluctuations in the upper soil layers were due to temperature fluctuations.

Methodological Issues

The O_2 optode sensor array has proven to have remarkable long-term stability. A spear array was inserted in the peat soil in November 2008 and was retrieved in December 2012; the 3-wk in situ data set reported here was obtained from the same spear deployment. From November 2008 to May 2009, the water level was at ground level, resulting in measurements showing anoxia at all 10 sensor depths. In December 2012, the spear array was removed from the measuring site. The retrieved sensor array was brought back to the laboratory, washed with water, and put in the water-filled calibration container. After more than 4 yr of deployment, 6 out of 10 sensors were still fully functional. The sensors at 20, 40, 50, 60, 70, and 80 cm were intact except for the black silicone coating, which was probably lost

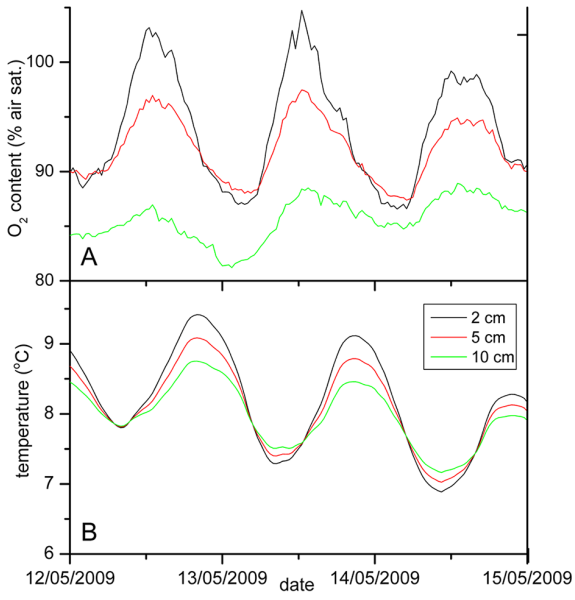

Fig. 5. A magnified representation of the dynamics of O_2 (A) and temperature (B) at depths of 2, 5, and 10 cm as measured over the first 3 d of the measuring period shown in Fig. 4. The water level decreased from 12 to 19 cm below ground level over the same period, and there was no precipitation.

during removal of the spear from the soil. The fact that the upper sensors of the array were lost is probably due to the much higher mechanical impact on these sensors during retrieval because they were tightly enclosed by the rhizomes of the vegetation. When recalibrated at 100% air saturation and 14.5°C, the phase angle of the six functional sensors had increased by 1.11 ± 0.45° relative to the original calibration value, corresponding to an apparent decrease in the measured O_2 content from 100 to 93.6%. The anoxic recalibration was performed at 15.4°C and showed an average decrease in the phase angle (relative to the original calibration before installation of the spear) of 1.18 ± 0.19°. This corresponds to an apparent increase in measured O_2 from 0 to 1.9% air saturation when referring to the original calibration.

In this study, we monitored the 10 optodes mounted in the spear with a 10-channel fiberoptic O_2 meter. Another possibility for using multiple sensors is to image the end of a fiber bundle with the O_2–sensing ends distributed in the sample (Fischer and Koop-Jakobsen, 2012); these authors used an expensive life-time imaging system for sensor read-out. Both the bundle approach and the spear approach presented here can be combined with ratiometric O_2 sensor readout using the inexpensive camera system of Larsen et al. (2011), and such work is in progress (Larsen et al., unpublished).

Conclusions

We present a new robust tool for spatially resolved in situ measurements of O_2 and temperature in soil and sediment undergoing changes in water level. The new sensor array device allows for simultaneous O_2 and temperature measurements at 10 depths in the soil horizon using a combination of fiberoptic O_2 sensors and thermocouples. Based on the linear response of O_2–dependent sensor luminescence to temperature, it is possible to correct sensor signals for fluctuating temperature. The long-term stability of optical O_2 sensors enabled in situ measurement in a peat soil for several months in combination with monitoring of water levels, temperature, and a range of other environmental data. This application illustrated the value of mapping O_2 conditions in wetlands at high spatiotemporal resolution in relation to water level fluctuations. The new device thus allows long-term in situ studies of O_2 dynamics, which is highly relevant for understanding the effects of water level changes on net greenhouse gas budgets in wetlands.

Future tests of the sensor array should include a more detailed analysis of sensor sensitivity with respect to total pressure variations, coating of secondary phases on the sensors, soil compaction around the array after installation, preferential root growth, and water flow along the spear.

Acknowledgments

This study was supported by grants from the Danish Natural Science Research Council (BE, RNG, MK), the Danish Research Council for Technology and Production (MK), and the Danish National Advanced Technology Foundation (MK). RNG was financially supported by the National Environmental Research Council (NERC)– NE/F018612/1; NE/F0122991/1, the Commission for Scientific Research in Greenland; KVUG; GCRC6507, EU; HYPOX-226213; and ERC advanced grant 2010-AdG_20100224. The authors thank Egil Nielsen with the mechanical construction of the sensor array and Christian Juncher Jørgensen for quality testing and managing the data base.

References

Askaer, L., B. Elberling, R.N. Glud, M. Kühl, F.R. Lauritsen, and H.P. Joensen. 2010. Soil heterogeneity effects on O_2 distribution and CH_4 emissions from wetlands: In situ and mesocosm studies with planar O_2 optodes and membrane inlet mass spectrometry. Soil Biol. Biochem. 42:2254–2265. doi:10.1016/j.soilbio.2010.08.026

Askaer, L., B. Elberling, T. Friborg, C.J. Jørgensen, and B.U. Hansen. 2011. Plant-mediated CH_4 transport and C gas dynamics quantified in-situ in a *Phalaris arundinacea*-dominant wetland. Plant Soil 343:287–301. doi:10.1007/s11104-011-0718-x

Boelter, D.H. 1965. Hydraulic conductivity of peats. Soil Sci. 100:227–231. doi:10.1097/00010694-196510000-00001

Daulat, W.E., and R.S. Clymo. 1998. Effects of temperature and water table on the efflux of methane from peat land surface cores. Atmos. Environ. 32:3207–3218. doi:10.1016/S1352-2310(98)00078-8

Elberling, B., L. Askaer, C.J. Jørgensen, H.P. Joensen, M. Kühl, R.N. Glud, and F.R. Lauritsen. 2011. Linking soil O_2, and CH_4 concentrations in a wetland soil: Implications for CO_2 and CH_4 fluxes. Environ. Sci. Technol. 45:3393–3399. doi:10.1021/es103540k

Fischer, J.P., and K. Koop-Jakobsen. 2012. The multi fiber optode (MufO): A novel system for simultaneous analysis of multiple fiber optic oxygen sensors. Sens. Actuators B 168:354–359. doi:10.1016/j.snb.2012.04.034

Glud, R.N. 2008. Oxygen dynamics of marine sediments. Mar. Biol. Res. 4:243–289. doi:10.1080/17451000801888726

Glud, R.N., I. Klimant, G. Holst, O. Kohls, V. Meyer, M. Kühl, and J.K. Gundersen. 1999. Adaptation, test and in situ measurements with O_2 microopt(r)odes on benthic landers. Deep-Sea Res. 46:171–183. doi:10.1016/S0967-0637(98)00068-5

Hargreaves, K.J., and D. Fowler. 1998. Quantifying the effects of water table and soil temperature on the emission of methane from peat wetland at the field scale. Atmos. Environ. 32:3275–3282. doi:10.1016/S1352-2310(98)00082-X

Hecht, H., and M. Kölling. 2001. A low-cost optode array measuring system based on 1 mm plastic optical fibers: New technique for in situ detection and quantification of pyrite weathering processes. Sens. Actuators B 81:76–82. doi:10.1016/S0925-4005(01)00934-0

Holst, G., M. Kühl, and I. Klimant. 1995. A novel measuring system for oxygen microoptodes based on a phase modulation technique. Proc. SPIE 2508:387–398. doi:10.1117/12.221754

Holst, G., R.N. Glud, M. Kühl, and I. Klimant. 1997. A microoptode array for fine scale measurements of oxygen distribution. Sens. Actuators B 38:122–129. doi:10.1016/S0925-4005(97)80181-5

Holst, G., I. Klimant, O. Kohls, and M. Kühl. 2000. Optical microsensors and microprobes. In: M. Varney, editor, Chemical sensors in oceanography. Gordon & Breach, New York. p. 143–188.

Ingram, H.A.P. 1983. Hydrology. In: A.J.P. Gore, editor, Mires: Swamp, bog, fen and moor. General studies. Ecosystems of the World. Vol. 4A. Elsevier, New York.

IPCC. 2007. IPCC climate change 2007: Synthesis report. Contribution of Working Groups I, II and III to the Fourth Assessment Report of the Intergovernmental Panel on Climate Change. R.K. Pachauri. and A. Reisinger, editors. IPCC, Geneva, Switzerland.

Jørgensen, C.J., S. Struwe, and B. Elberling. 2012. Temporal trends in N_2O flux dynamics in a Danish wetland: Effects of plant-mediated gas transport of N_2O and O_2 following changes in water level and soil mineral-N availability. Glob. Change Biol. 18:210–222. doi:10.1111/j.1365-2486.2011.02485.x

Kettunen, A. 2003. Connecting methane fluxes to vegetation cover and water table fluctuations at microsite level: A modelling study. Global Biogeochem. Cycles 17:1051–1070. doi:10.1029/2002GB001958

Klimant, I., V. Meyer, and M. Kühl. 1995. Fiber-optic oxygen microsensors, a new tool in aquatic biology. Limnol. Oceanogr. 40:1159–1165. doi:10.4319/lo.1995.40.6.1159

Kölling, M., H. Hecht, and G. Holst. 2002. Simple plastic fiber based optode array for the in-situ measurement of the ground air oxygen concentrations. In: T. Vo-Dinh and S. Büttgenbach, editors, Advanced environmental sensing technology II. SPIE Proceedings 4576:75–86.

Kühl, M. 2005. Optical microsensors for analysis of microbial communities. Methods Enzymol. 397:166–199. doi:10.1016/S0076-6879(05)97010-9

Kühl, M., and L. Polerecky. 2008. Functional and structural imaging of phototrophic microbial communities and symbioses. Aquat. Microb. Ecol. 53:99–118. doi:10.3354/ame01224

Larsen, M., S.M. Borisov, B. Grünwald, I. Klimant, and R.N. Glud. 2011. A simple and inexpensive high resolution color ratiometric planar optode imaging approach: Application to oxygen and pH sensing. Limnol. Oceanogr. Methods 9:348–360. doi:10.4319/lom.2011.9.348

Liengaard, L., L.P. Nielsen, N.P. Revsbech, B. Elberling, A. Priemé, A.E. Prast, and M. Kühl. 2013. Extreme emission of N_2O from tropical wetland soil (Pantanal, South America). Front. Microbiol. 3:433. doi:10.3389/fmicb.2012.00433

Macdonald, J.A., D. Fowler, K.J. Hargreaves, U. Skiba, L.D. Leith, and M.B. Murray. 1998. Methane emission rates from a northern wetland; Response to temperature, water table and transport. Atmos. Environ. 32:3219–3227. doi:10.1016/S1352-2310(97)00464-0

Megonigal, J.P., M.E. Hines, and P.T. Visscher. 2003. Anaerobic metabolism: Linkages to trace gases and aerobic processes. In: H.D. Holand and K.K. Turekian, editors, Treatise on geochemistry. Vol. 8. Elsevier, New York. p. 317–424.

Schäfer, C.-M., L. Elsgaard, C.C. Hoffmann, and S.O. Petersen. 2012. Seasonal methane dynamics in three temperate grasslands on peat. Plant Soil 357:339–353. doi:10.1007/s11104-012-1168-9

Schwärzel, K., M. Renger, R. Sauerbrey, and G. Wessolek. 2002. Soil physical characteristics of peat soils. J. Plant Nutr. Soil Sci. 165:479–486. doi:10.1002/1522-2624(200208)165:4<479::AID-JPLN479>3.0.CO;2-8

Uchida, H., T. Kawano, I. Kaneko, and M. Fukasawa. 2008. In situ calibration of optode-based oxygen sensors. J. Atmos. Ocean. Technol. 25:2271–2281. doi:10.1175/2008JTECHO549.1